Modelling Geomagnetically Induced Currents

Article *in* Space Weather · December 2016

DOI: 10.1002/2016SW001499

CITATIONS
103

READS
1,185

2 authors:

David Boteler
Natural Resources Canada
182 PUBLICATIONS **3,822** CITATIONS
SEE PROFILE

Risto Pirjola
Finnish Meteorological Institute
174 PUBLICATIONS **6,167** CITATIONS
SEE PROFILE

AGU PUBLICATIONS

Space Weather

RESEARCH ARTICLE
10.1002/2016SW001499

Special Section:
NASA's Living With a Star: Geomagnetically Induced Currents

Modeling geomagnetically induced currents

D. H. Boteler[1] and R. J. Pirjola[1,2]

[1]Geomagnetic Laboratory, Natural Resources Canada, Ottawa, Ontario, Canada, [2]Finnish Meteorological Institute, Helsinki, Finland

Abstract Understanding the geomagnetic hazard to power systems requires the ability to model the geomagnetically induced currents (GIC) produced in a power network. This paper presents the developments in GIC modeling starting with an examination of fundamental questions about where the driving force for GIC is located. Then we outline the two main network modeling approaches that are mathematically equivalent and show an example for a simple circuit. Accurate modeling of the GIC produced during real space weather events requires including the appropriate system characteristics, magnetic source fields, and Earth conductivity structure. It is shown how multiple voltage levels can be included in GIC modeling and how the network configuration affects the GIC values. Magnetic source fields can be included by using "plane wave" or line current models or by using geomagnetic observatory data with an appropriate interpolation scheme. Earth conductivity structure can be represented by 1-D, 2-D, or 3-D models that are used to calculate the transfer function between electric and magnetic fields at the Earth's surface. For 2-D and 3-D structures this will involve a tensor impedance function and electric fields that are not necessarily orthogonal to the magnetic field variations. It is now technically possible to include all these features in the modeling of GIC, and various software implementations are being developed to make these features more accessible for use in risk studies.

Key Points:
- GIC modeling can now include geomagnetic disturbance characteristics and Earth conductivity to calculate GIC throughout a power system
- Inclusion of geomagnetic disturbance characteristics and 3-D Earth conductivity structure in GIC modeling is often limited by lack of data
- GIC modeling has a high state of application readiness and is used for hazard assessments and real-time geomagnetic disturbance management

Correspondence to:
D. H. Boteler,
david.boteler@canada.ca

Citation:
Boteler, D. H., and R. J. Pirjola (2017), Modeling geomagnetically induced currents, *Space Weather*, *15*, 258–276, doi:10.1002/2016SW001499.

Received 12 AUG 2016
Accepted 11 DEC 2016
Accepted article online 15 DEC 2016
Published online 31 JAN 2017

1. Introduction

A major threat from space weather to critical infrastructure is the effect of geomagnetic disturbances on power systems. Assessing the geomagnetic risk to power systems requires understanding geomagnetic field variations, the influence of Earth conductivity structure on the geoelectric fields that they induce, and the power system characteristics, which taken together determine the geomagnetically induced currents (GIC) that are produced in a power system. These GIC can then be used to determine the effects on transformers and subsequent effects on other power system components and on the operation of the power system itself. Many studies have been made of the geophysical and engineering aspects of this problem [see *Molinski*, 2002; *Kappenman*, 2007; *Pulkkinen et al*., 2016, and references therein]. However, central to geomagnetic risk assessments, and the subject of this paper, is the ability to model the GIC produced in a power system.

The first calculations of GIC were made using power system network modeling software [*Albertson et al*., 1981; *Kappenman et al*., 1981]. The first software designed for GIC modeling was developed by *Lehtinen and Pirjola* [1985]. Since then power network modeling has been used by the power industry, while the Lehtinen-Pirjola method has been mainly used by the geophysics community. Early studies involving GIC modeling were primarily made for high-latitude power systems in Finland [*Pirjola and Lehtinen*, 1985; *Mäkinen*, 1993] and Canada [*Boteler et al*., 1994]. Later, it was recognized that GIC could affect power systems all over the world and GIC studies were made in many countries. Specific studies that included modeling of GIC have been done for the UK [*Erinmez et al*., 2002; *McKay*, 2003; *Turnbull*, 2010, 2011; *Kelly et al*., 2016]; the U.S. [*Radasky et al*., 2006; *Arajärvi and Viljanen*, 2008; *Gilbert et al*., 2012; *Bernabeu*, 2013]; South Africa [*Koen*, 2002; *Bernhardi et al*., 2008; *Ngwira et al*., 2008; *Taylor et al*., 2014]; Sweden [*Wik et al*., 2008]; Norway [*Myllys et al*., 2014]; Spain [*Torta et al*., 2014]; northern, central, and southern Europe [*Viljanen et al*., 2012, 2014]; France [*Kelly et al*., 2016]; Australia [*Marshall et al*., 2011]; New Zealand [*Marshall et al*., 2012]; Brazil [*Barbosa et al*., 2015]; Uruguay [*Caraballo et al*., 2013]; and China [*Zheng et al*., 2012; *Liu et al*., 2013, 2014; *Guo et al*., 2015].

GIC modeling often uses a uniform electric field as input to a network model, which in early studies comprised transmission lines and single resistances representing the combined paths to ground through each substation, although a study including two voltage levels was already made by *Mäkinen* [1993]. Now GIC calculations involve transmission lines at different voltage levels and the resistances of individual

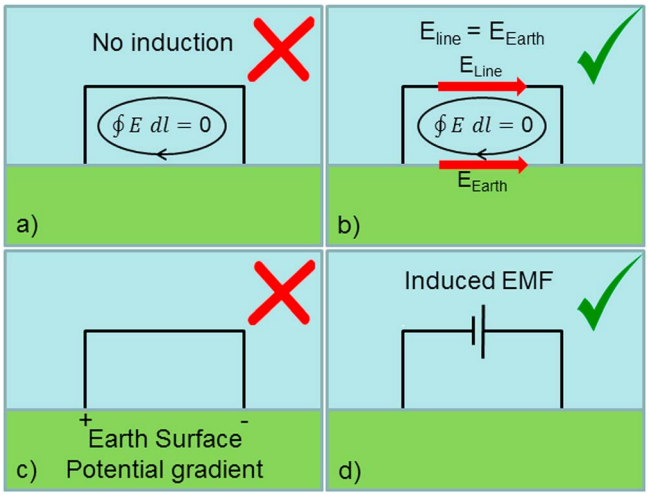

Figure 1. Views of geomagnetic induction in power systems. (a) Incorrect and (b) correct views of the integral of electric field around loop formed by a power line and the Earth's surface equal to 0. (c) Incorrect and (d) correct views of the driving force for GIC in a power system.

transformers as well as including characteristics of the geomagnetic source fields and Earth conductivity structure. The ultimate aim is to accurately simulate the GIC produced by real space weather events. This paper illustrates the development of GIC modeling and examines the current state of the art. First, we consider fundamental aspects of GIC modeling, present the methodology for modeling GIC given specified electric fields as inputs, and examine how power system characteristics affect GIC. Then we consider how the characteristics of geomagnetic disturbances and the conductivity structure of the Earth influence the GIC calculations. Finally, we consider how GIC modeling can be integrated into studies of the geomagnetic hazard to power systems.

2. Fundamentals

There has been a lot of confusion about how geomagnetic disturbances actually drive GIC. Faraday's law can be used to relate the electric field integrated round the loop formed by a power line, connections to ground at the ends, and return path along the Earth's surface to the rate of change of the magnetic flux through the loop (Figures 1a and 1b). However, simple calculations show that at GIC frequencies the rate of change of magnetic flux is very small giving an electric field integrated round the loop that is not large enough to drive the GIC that are observed. For example, consider the loop formed by a power line 200 km long at a height of 30 m and the Earth's surface, with a sinusoidally varying magnetic field through the loop with an amplitude of 2000 nT and period of 5 min. Using Faraday's law, this gives an electric field integrated round the loop of only 0.25 V. (In comparison, using (11) for a uniform Earth with 1000 Ω m resistivity gives an integrated electric field of 1633 V.) The fact that the integral round the power line—Earth surface loop being essentially 0 is sometimes mistakenly taken to mean that there is no induction at all (Figure 1a). Instead, the induction involves a loop extending down into the Earth (see section 2.1) and the zero integral round the loop formed by the transmission line and Earth surface shows that the electric field in the transmission line has the same magnitude and direction as the electric field along the Earth's surface (Figure 1b).

An alternative view, used by early researchers, is based on the fact that electric currents flow in the Earth during geomagnetic disturbances and there would be an "IR drop" associated with the energy loss of this current. This was interpreted as producing an Earth surface potential gradient that would drive GIC from the Earth up into the power system (Figure 1c). However, the geomagnetic field variations produce an induced electromotive force (emf) in both the Earth and the power lines. In the Earth the induced emf drives a current, and there is an IR voltage drop associated with this current flow, but these are distributed so that in a uniform or layered Earth, in any chosen length the induced emf and IR voltage drop exactly match so that the current is driven purely by the induced emf with no potential gradients in the Earth. Thus, with a uniform or layered Earth, there are no potential differences between the grounding points of the power system and GIC are driven by the induced emf in the transmission lines (Figure 1d) which acts like an extra voltage source in the line Vab = $E_0 \times l$, where E_0 is the horizontal component of the induced geoelectric field along the direction of the line of length, l

2.1. Calculation of Electric Fields

The next question is as follows: how do we calculate the induced emf in a transmission line of a power system? The theory for electromagnetic induction starts with Maxwell's equations, which can be used either in their integral form or in their derivative form to give expressions for diffusion of the fields into the Earth. To

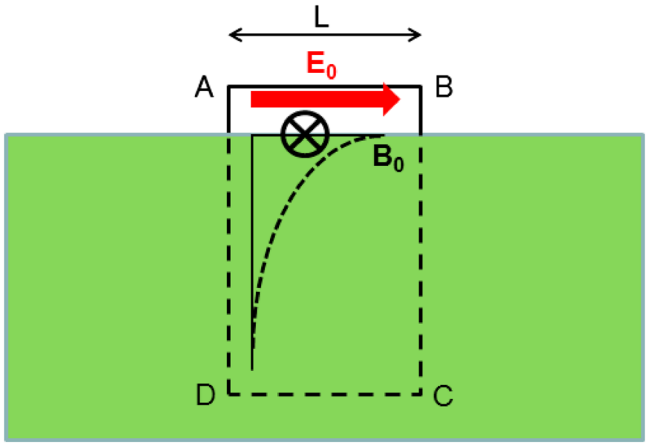

Figure 2. Geomagnetic induction in the loop ABCD.

illustrate the fundamentals, we will consider induction in a power line at the surface of an Earth with uniform conductivity [see *Boteler*, 1999]. (The influence of realistic Earth conductivity structure on GIC will be considered in a later section.) We use a geographic coordinate system where *x* points north, *y* points east, and *z* is directed vertically downward.

The magnetic field variations relevant to GIC span the frequency range from 10^{-5} to 1.0 Hz: at lower frequencies the variations are too slow to produce significant GIC, while at higher frequencies the power system inductances will have a damping effect. Therefore, starting with Maxwell's equations in the derivative form, we can drop the displacement current term as being negligible, i.e., $\sigma \gg \omega\epsilon_0$, for the Earth conductivities and frequencies range specified, and use Ohm's law with scalar conductivity, σ. Assuming a time variation of the form $e^{j\omega t}$, and using the magnetic permeability of free space, $\mu_0 = 4\pi 10^{-7}$H/m, these can be written

$$\nabla \times \boldsymbol{E} = -j\omega \boldsymbol{B} \tag{1}$$

$$\nabla \times \boldsymbol{B} = \mu_0 \sigma \boldsymbol{E} \tag{2}$$

Taking the curl of (1) and substituting into (2) gives the diffusion equation

$$\nabla^2 \boldsymbol{E} = j\omega\mu_0\sigma \boldsymbol{E} \tag{3}$$

where σ is the uniform Earth conductivity. For electric fields with horizontal variations that are much less than the variation with depth equation (3) has a solution of the form

$$E = E_0 e^{-z/p} \tag{4}$$

where E_0 is the amplitude of the electric field at the Earth = *s* surface, and *p* is the complex skin depth:

$$p = 1/\sqrt{j\omega\mu_0\sigma} \tag{5}$$

Substituting *E* from (4) back into equation (1) gives the transfer function of the Earth, *K*, relating the orthogonal surface electric and magnetic fields for a downward propagating wave in the *z* direction with transverse *E* and *B* fields.

$$K = -\frac{E_0}{B_0} = \left(\frac{j\omega}{\mu_0\sigma}\right)^{1/2} \tag{6}$$

where *K* is related to the magnetotelluric surface impedance, *Z*, and the complex skin depth, *p*,

$$K = \frac{Z}{\mu_0} = j\omega\ p \tag{7}$$

Alternatively, consider the power line AB, with length *L*, shown in Figure 2. The surface electric and magnetic fields are designated by E_0 and B_0 as before. Consider a vertical loop extending to infinity below the power line, shown by the dashed lines BC, CD, and DA in Figure 2. The magnetic field within the loop ABCD has a value B_0 at the surface and falls off exponentially below the surface

$$B = B_0 e^{-z/p} \tag{8}$$

The magnetic flux through the loop ABCD is then found by integrating equation (8) for depths *z* from 0 to infinity and multiplying by the length *L*:

$$\Phi = \int_0^\infty B\ \mathrm{d}zL = pB_0L \tag{9}$$

As stated by Faraday's law, the electric field integrated round the loop ABCD is then given by the negative rate of change of the magnetic flux through the loop ABCD

$$\oint_{ABCD} E \ \mathrm{d}l = -\frac{\mathrm{d}\Phi}{\mathrm{d}t} = -j\omega p B_0 L \tag{10}$$

The electric field is horizontal, so there will be no electric field along sides BC or DA of the loop. Also, the electric field drops to 0 at infinity, where the loop closes along section CD. Thus, the integral around loop ABCD is given by the electric field integrated along the side AB which is given by $E_0 L$. Thus, dividing both sides of equation (10) by L gives the electric field

$$E_0 = -j\omega p B_0 \tag{11}$$

which can be seen to give the same relation, K, between electric and magnetic fields at the Earth's surface as equation (7). Thus, the "diffusion equation" approach and Faraday's law approach both give the same results as long as the right loop is considered when using Faraday's law.

The above calculations have been for a power system that is away from conductivity boundaries in the Earth, and the only driving force is the emf induced by the magnetic field variation. For such a situation it can be shown that the geomagnetic induction process will not produce any accumulation of charge and hence no potential gradients at the Earth's surface [*Boteler and Pirjola*, 1997]. However, when the Earth has lateral variations in conductivity, this not only changes the amplitudes of the electric fields but also affects the nature of the electric fields. In general, an electric field is composed of two parts: one involving the vector potential, **A**, and the other involving the scalar potential, Φ:

$$E = -\frac{\partial \mathbf{A}}{\partial t} - \nabla\Phi \tag{12}$$

For calculations of the electric field produced during geomagnetic disturbances we use Maxwell's equations which are written in terms of the total electric field, so any information about the vector and scalar potential composition of the electric field is not immediately obvious. However, Maxwell's equations involve the curl and divergence of the electric field. In taking the curl of the electric field in equation (12) the scalar potential term gives 0, so the curl of the electric field only comes from the vector potential part. Contrastingly, in taking the divergence of the electric field the divergence of the vector potential part can be set to 0 so that the divergence of the electric field comes only from the scalar potential part. Thus, in general, an electric field is composed of a vector potential term produced by a changing magnetic field and a scalar potential term due to a distribution of charge. The distribution of charge occurs at conductivity boundaries such as coastlines and produces localized electric fields in addition to the primary induced emf produced by the magnetic field variations.

2.2. Including Electric Fields in Network Models

The final fundamental aspect of GIC modeling is how to include the electric fields in the network model. The full details of modeling complex networks will be considered in the next section. To illustrate the fundamentals of including electric fields, it is useful to consider a simple square network as used by *Boteler and Pirjola* [1998a] to show why realistic (nonuniform) electric fields must be represented by voltage sources in the lines and not by voltage sources at the grounding connections of the network. Some earlier studies had used voltage sources at the grounding connections to represent an Earth surface potential gradient. Although this is physically incorrect, it is curious that these studies gave the correct GIC results for a uniform electric field. In many cases a uniform field is a useful simplifying assumption; however, *Boteler and Pirjola* [1998a] show that a uniform field is a mathematical oddity in that it does not have the same properties as a realistic field that goes to 0 at infinity. Their analysis showed that voltage sources in the transmission lines or at the grounding connections both give correct GIC results in the special case of a uniform electric field. However, for realistic electric fields (i.e., produced by nonuniform source fields), only voltage sources in the transmission lines can accurately represent the electric fields and hence give the correct GIC values.

The above analysis only considered nonuniformity of the electric fields arising from spatial structure of the source magnetic field variations. However, nonuniform electric fields can also occur as a result of localized electric field enhancements arising from spatial structure in the Earth conductivity. To examine this, we use the simple network model of *Boteler and Pirjola* [1998a] placed in the vicinity of a coast line (Figure 3).

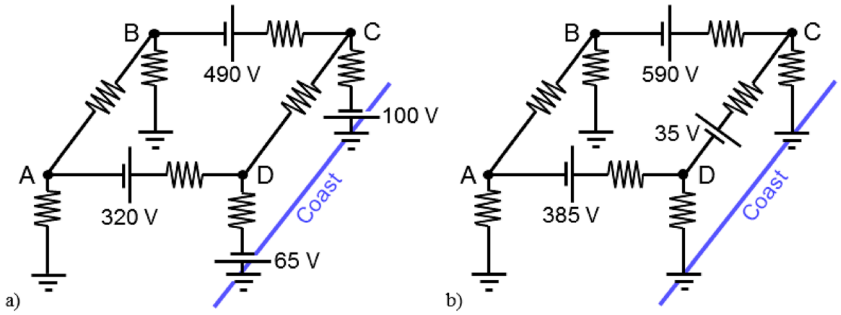

Figure 3. Geomagnetic induction in a square network next to the coast. The line resistances are 5 ohm, and the substation resistances are 0.5 ohm. Electric fields represented by (a) a combination of voltage sources in the lines and at the ground points or (b) voltage sources in the lines.

The network consists of four substations, each with a resistance (through transformer windings) to ground of 0.5 ohm, connected by 100 km long transmission lines each with a resistance of 5 ohm. The same line current source as in *Boteler and Pirjola* [1998a] is assumed as the primary driver giving induced emfs which vary with distance from the source giving electric fields of 4.9 V/km and 3.2 V/km in lines BC and AD, respectively. For these 100 km lines these electric fields can be represented by voltage sources in the lines of 490 V and 320 V as shown in Figure 3a. However, with the proximity of the network to the coast there is now an additional electric field at the coast. This is assumed to increase the electric field by a factor of 1.2 at each location. This can be represented by voltage sources of 100 V and 65 V at the "coastal" substations C and D, respectively (as in Figure 3a), or by addition of these amounts to the voltage sources in the transmission lines as shown in Figure 3b. Calculations of GIC with each set of sources give the same results (see Table 1). It is easier to deal with one set of voltage sources, and only the voltage sources in the lines can represent electric fields that have both a rotational and a conservative component [*Boteler and Pirjola*, 1997]. Thus, only voltages in the lines can be used for modeling GIC for realistic cases.

3. Network Modeling

Calculations of GIC can be made by setting up a network model of the system impedances. Voltage sources, calculated by integrating the electric field along each transmission line, are the input to this model. At the frequencies normally considered in GIC studies the reactive impedances are assumed to be negligible and the system is modeled as a network of resistances. (The validity of this assumption will be considered in section 7.) The power system consists of transmission lines and transformer windings for each phase of the three-phase system. These phase conductors provide identical parallel paths for GIC flow. Thus, GIC calculations can be made for a single phase only, knowing that the same results will apply to the other two phases. Using a resistive network, application of Kirchhoff's voltage law for each loop leads to a mesh impedance matrix equation that can be solved to give the currents in each loop [*Boteler*, 2014]. However, this method is not efficient for large networks in which case it is better to describe the system as a network of admittances.

Table 1. Model Results of GIC Produced by an Electric Field Due To an Ionospheric Line Current in a Square Network Next to the Coast, Showing That Representing the Coast Effect by Voltage Sources at the Ground Points (Figure 3a) or Including it in the Voltage Sources in the Lines (Figure 3b) Gives the Same Results

Location	GIC (Using Figure 3a)	GIC (Using Figure 3b)
A to ground	−67.0	−67.0
B to ground	−95.5	−95.5
C to ground	101.3	101.3
D to ground	61.2	61.2
A to B	2.8	2.8
A to D	64.2	64.2
B to C	98.3	98.3
C to D	−3.0	−3.0

To represent the production of GIC in a power system using an admittance network, each resistive branch is replaced by its corresponding admittance value and the voltage sources, e, are replaced by equivalent current sources, $j = e/r_L$ in parallel with the transmission line admittance $y_L = 1/r_L$. where r_L is the transmission line resistance.

Kirchhoff's current law is then used for each node in the network to give a set of equations relating the currents and nodal voltages to the current sources at each node.

$$j_k = i_k + v_k \sum_{n=1}^{N} y_{nk} - \sum_{n=1}^{N} v_n y_{nk} \tag{13}$$

This equation involves the nodal voltages v_k and currents to ground i_k as unknowns; however, these are related by Ohm's law

$$i_k = v_k y_k \tag{14}$$

So equation (14) can be substituted into equation (13) to give equations with only the nodal voltages or the currents as the unknowns.

In the nodal admittance matrix (NAM) method equations (13) and (14) are combined to give equations involving the nodal voltages. The voltages of the nodes are then found by taking the inverse of the admittance matrix and multiplying by the nodal current sources

$$[V] = [Y]^{-1}[J] \tag{15}$$

where $[J]$ is the current source vector with elements given by summing the current sources directed into each node

$$J_k = \sum_{n=1}^{N} j_{nk} \tag{16}$$

and $[Y]$ is the admittance matrix in which the diagonal elements are the sums of the admittances of all paths connected to node k, and the off-diagonal elements are the negative admittances of the connections between nodes k and n, i.e.,

$$\begin{aligned} Y_{kk} &= y_k + \sum_{n=1}^{N} y_{nk} \qquad n \neq \mathrm{k} \\ Y_{nk} &= -y_{nk} \end{aligned} \tag{17}$$

The calculated nodal voltages can then be substituted into (14) to give the currents to ground from each node.

The Lehtinen-Pirjola (LP) method combines equations (13) and (14) to give equations involving the currents to ground that are solved by matrix inversion.

$$[I^e] = ([1] + [Y^n][Z^e])^{-1}[J^e] \tag{18}$$

where [1] is the identity matrix, and the admittance matrix $[Y^n]$ is given by

$$\begin{aligned} Y^n_{kk} &= \sum_{n=1}^{N} y_{nk} \qquad n \neq \mathrm{k} \\ Y^n_{kn} &= -y_{kn} \end{aligned} \tag{19}$$

$[Z^e]$ is the earthing impedance matrix relating the currents to ground from each node to the nodal voltages

$$v_k = \sum_{n=1}^{N} Z^e_{kn} i_n \tag{20}$$

and the current source vector is given by (16)

The currents to ground obtained by the Lehtinen-Pirjola method can also be used with (14) to give the nodal voltages. The nodal voltages, obtained by either technique, can then be used to give the currents in other branches in the network:

$$i_{nk} = j_{nk} + (v_n - v_k) y_{nk} \tag{21}$$

Comparison of the NAM and LP methods [*Boteler and Pirjola*, 2014] shows that the two methods are mathematically equivalent.

3.1. Example Calculation

The modeling can be illustrated by considering the network shown in Figure 3b. Converting this to an admittance network results in the circuit of Figure 4. The substation names A, B, C, and D have been replaced with node numbers 1, 2, 3, and 4.

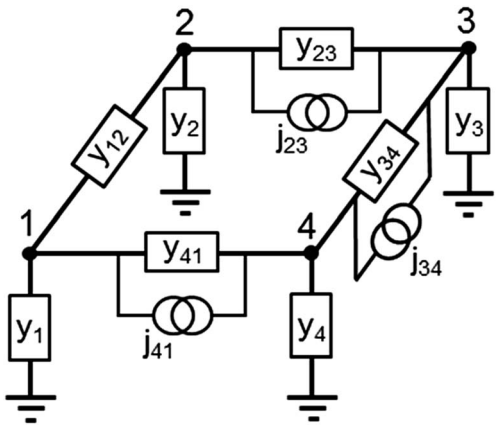

Figure 4. Single-phase diagram of the simple power network of Figure 3b represented by admittances, *y*, and equivalent current sources, *j*.

For the nodal admittance network, at each node apply Kirchhoff's current law that the algebraic sum of the currents entering any node is 0, i.e., the sum of currents entering on transmission lines equals current flowing to ground. Applying this to the network in Figure 4 gives equations for each node

$$\begin{aligned} i_{41} - i_{12} &= i_1 \\ i_{12} - i_{23} &= i_2 \\ i_{23} - i_{34} &= i_3 \\ i_{34} - i_{41} &= i_4 \end{aligned} \tag{22}$$

The current in a line is determined by the current source, the voltage difference between nodes at the ends of the line, and the admittance of the line

$$i_{nk} = j_{nk} + (v_n - v_k) y_{nk} \tag{23}$$

Note that $i_{nk} = -i_{kn}$ and $y_{nk} = y_{kn}$. Also, using Ohm's law, the current flowing to ground from each node can be written in terms of the nodal voltage

$$i_k = y_k v_k \tag{24}$$

Substituting for the currents in the equations above, we obtain equations involving just the voltages of each node as the unknowns:

$$\begin{aligned} j_{41} + y_{41}(v_4 - v_1) - j_{12} - y_{12}(v_1 - v_2) &= y_1 v_1 \\ j_{12} + y_{12}(v_1 - v_2) - j_{23} - y_{23}(v_2 - v_3) &= y_2 v_2 \\ j_{23} + y_{23}(v_2 - v_3) - j_{34} - y_{34}(v_3 - v_4) &= y_3 v_3 \\ j_{34} + y_{34}(v_3 - v_4) - j_{41} - y_{41}(v_4 - v_1) &= y_4 v_4 \end{aligned} \tag{25}$$

Rearranging gives

$$\begin{aligned} j_{41} - j_{12} &= -y_{41} v_4 + (y_{41} + y_1 + y_{12}) v_1 - y_{12} v_2 \\ j_{12} - j_{23} &= -y_{12} v_1 + (y_{12} + y_2 + y_{23}) v_2 - y_{23} v_3 \\ j_{23} - j_{34} &= -y_{23} v_2 + (y_{23} + y_3 + y_{34}) v_3 - y_{34} v_4 \\ j_{34} - j_{41} &= -y_{34} v_3 + (y_{34} + y_4 + y_{41}) v_4 - y_{41} v_1 \end{aligned} \tag{26}$$

The current sources in parallel with the line from node *k* to node *n* can be represented by "nodal current sources" at each end of the line: one pulling current out of node *k* and one injecting current into node *n*. The currents on the left-hand side of (26) represent the total of the equivalent source currents directed into each node, which we term J_k. Thus, we can rewrite the equations in the form

$$\begin{aligned} J_1 &= -y_{41} v_4 + (y_{41} + y_1 + y_{12}) v_1 - y_{12} v_2 \\ J_2 &= -y_{12} v_1 + (y_{12} + y_2 + y_{23}) v_2 - y_{23} v_3 \\ J_3 &= -y_{23} v_2 + (y_{23} + y_3 + y_{34}) v_3 - y_{34} v_4 \\ J_4 &= -y_{34} v_3 + (y_{34} + y_4 + y_{41}) v_4 - y_{41} v_1 \end{aligned} \tag{27}$$

These equations can be written in matrix form

$$\begin{bmatrix} J_1 \\ J_2 \\ J_3 \\ J_4 \end{bmatrix} = \begin{bmatrix} y_{41} + y_1 + y_{12} & -y_{12} & 0 & -y_{41} \\ -y_{12} & y_{12} + y_2 + y_{23} & -y_{23} & 0 \\ 0 & -y_{23} & y_{23} + y_3 + y_{34} & -y_{34} \\ -y_{41} & 0 & -y_{34} & y_{34} + y_4 + y_{41} \end{bmatrix} \begin{bmatrix} v_1 \\ v_2 \\ v_3 \\ v_4 \end{bmatrix} \tag{28}$$

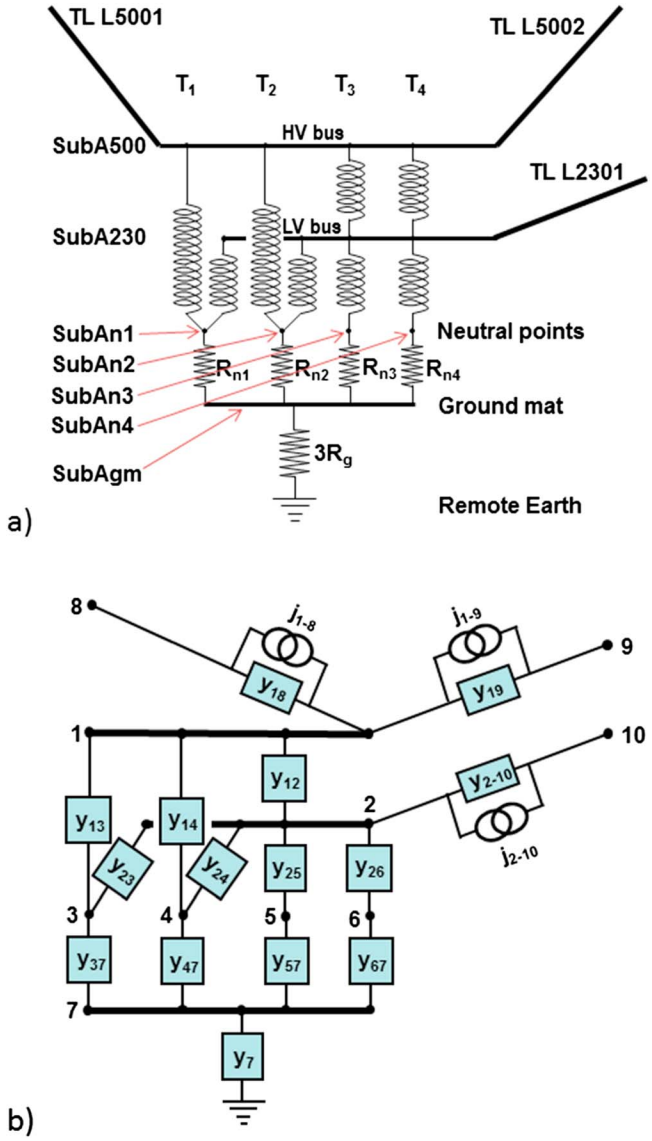

Figure 5. (a) Single-phase circuit diagram for a substation with two-winding transformers (T1 and T2) and autotransformers (T3 and T4) connected to transmission lines (TL) at 500 kV (L5001 and L5002) and at 230 kV (L2301). (b) Equivalent single-phase admittance network with current sources in the transmission line branches.

Matrix inversion can be used to solve for the nodal voltages which are then substituted into (23) to obtain the currents in the lines and also combined with the admittances to ground (24) to give the currents flowing to ground.

3.2. Practical Issues

The previous sections describe the theory for the GIC model calculations. However, applying this in practice requires extensive work in assembling the admittance matrix for the network. Impedances of each phase of the power system are identical so the same values of GIC will flow in each phase. Therefore, calculations of GIC need to be made for only one network and the values used to calculate the GIC in all three phases. This is often done by combining the parallel paths of all three phases to produce an equivalent circuit for calculating the total GIC in all three phases. To give the values for this equivalent circuit, the line resistances and transformer winding resistances need to be divided by 3. The path from the substation ground mat to remote Earth carries the GIC from all three phases, so the substation grounding resistance is the appropriate value to use. Alternatively, the calculations can be made for a single-phase network to give the GIC in amperes per phase. For this network all the resistance values will be 3 times those of the combined equivalent circuit; i.e., the actual line resistances and transformer winding resistances are used, while the substation grounding resistance is multiplied by 3. Use of this single-phase circuit is recommended as it gives the GIC in A per phase which are the values needed for assessing transformer saturation.

Figure 5a shows the single-phase circuit for a substation with transmission lines (L5001, L5002, and L2301) at voltage levels 500 kV and 230 kV connecting to other substations. Within the substation there are four transformers: two 2-winding transformers (T1 and T2) and two autotransformers (T3 and T4), each with a neutral point that is connected to the ground mat of the substation. The admittance network for the substation is shown in Figure 5b. Within this network the substation ground mat is the only node that is grounded, through admittance y_7. The rest of the admittances are branches within the network. The branches that represent transmission lines affected by the geoelectric field also have an equivalent current source in parallel, while those branches within a substation, such as transformer windings, do not. In this network model, nodes have also been added at the neutral point of each transformer. In many cases the neutral point may be solidly connected to the ground mat, but

including these as distinct connections in the model allows for the possibility of inserting neutral-ground resistors or capacitors.

In the original use of the Lehtinen-Pirjola (LP) method for a single voltage level and where substation resistances were lumped together to give a resistance to ground, each substation was represented by a single node and all nodes were connected to a local ground. Now with multiple voltages and the inclusion of separate neutral points, as in Figure 5, many of the nodes are ungrounded. In the LP method this would require an earthing impedance matrix with infinite values and the currents to ground from these nodes would be 0. In practice, the ungrounded nodes have a resistance to ground set to a high value (of the order of 10^{10} ohm) and the model calculations give values for the current to ground from these nodes that are very small (of the order of 10^{-10} A) rather than 0. This combination of high resistance and small current does then enable calculation of sensible values for the nodal voltages that are needed to calculate the currents in the rest of the network.

Resistance values for network components like transmission lines and transformers are not included in standard power system load flow calculations, so additional work will be needed to extract these values from data sheets. This is generally the most time-consuming part of setting up a GIC network model for a power system. If the power network is isolated, either geographically or electrically, then the network model is complete and can be used to calculate GIC. However, where a power system "A" is connected to neighboring networks "B" and "C" it is necessary to consider the GIC that may flow to/from these networks instead of flowing to ground through transformers at the edge of network "A." Ideally, the model could be extended to include all of networks "B" and "C," but this may not be practical. In such a situation, rather than ignore the neighboring networks completely, it is preferable to use an equivalent circuit for a neighboring network as shown by *Boteler et al*. [2013].

GIC produced in a power system are dependent on many factors: the system characteristics, the geomagnetic source fields, and the Earth conductivity structure that all combine to determine the GIC that occurs at any particular place and time. All of these factors need to be included for accurate modeling of the GIC that will occur. However, valuable insight into the influence of each factor can be gained by considering them individually. To do this, start by making calculations with a uniform electric field: this is a good first step as it does not require the extra information needed to calculate realistic electric fields and it is useful for examining how the system characteristics influence the flow of GIC (see next section). The network modeling process allows for different electric fields in each transmission line. Spatial variations in the electric fields arise due to both the geomagnetic source fields and the Earth conductivity structure. How these are included in GIC modeling is examined in the following sections.

4. Effect of System Characteristics

The fundamental system characteristics that influence the sizes of GIC are the resistances of system components. Because of the line construction used for different voltage levels, higher-voltage lines have lower resistance so experience the largest GIC [*Kappenman*, 2007; *Zheng et al*., 2014]. Thus, many studies have only considered the highest voltage level when modeling GIC. The first study to consider two voltage levels (400 kV and 220 kV) was done by *Mäkinen* [1993] for the Finnish power network [see also *Pirjola*, 2005]. More recently, the theory for modeling multiple voltage levels has been examined [*Boteler and Pirjola*, 2014] and two voltage levels were included in the Benchmark model of *Horton et al*. [2012]. The following question remains: how much do we need to include a lower voltage network in the modeling if we are only interested in GIC in a higher-voltage system? GIC in individual lower voltage lines will be smaller, but there may be more lines at the lower voltage, and so the total GIC could be comparable to the GIC in higher-voltage lines. Also, the lower voltage lines may provide a path for GIC from higher-voltage lines that may otherwise flow to ground at the end of the high voltage lines. *Torta et al*. [2014] examine the errors introduced in the Benchmark model calculations by leaving out the lower voltage level and found that GIC in the upper voltage level could be changed by up to 200%. However, as they point out, the effect of ignoring lower voltage levels will depend on the particular details of each system. *Guo et al*. [2015] investigate the effect of the extrahigh-voltage (500 kV) grid on GIC in the ultrahigh-voltage (1000 kV) system in China and show that the effect is significant.

A relation between GIC and line length has been reported in a number of papers. However, this is not a simple relationship. To illustrate this, *Zheng et al*. [2014] used the circuit in Figure 6a and obtained the dependence of GIC on voltage level and line length shown in Figure 6b. As well as showing larger GIC values for higher-

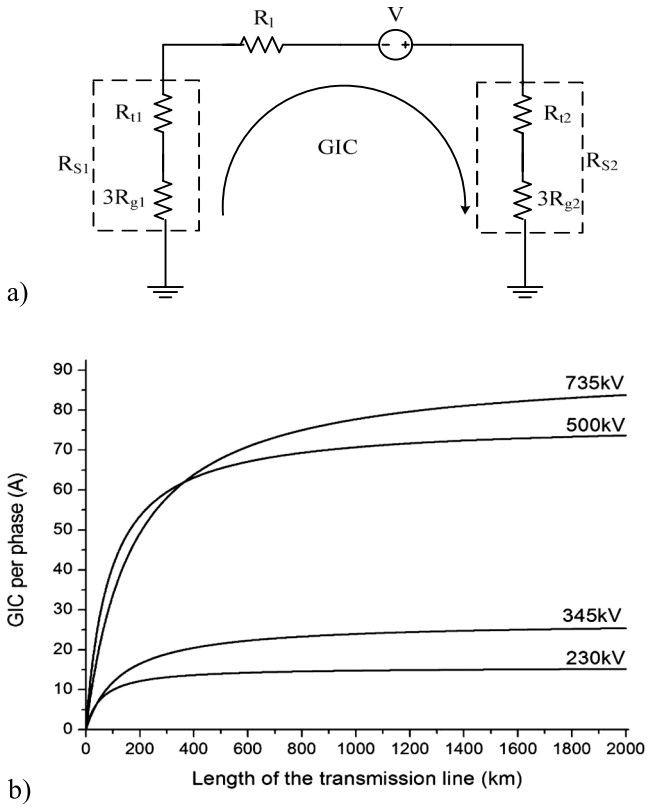

Figure 6. Dependence of GIC on line length [from *Zheng et al.*, 2014]. (a) Example circuit showing a transmission line connecting two substations. (b) GIC produced in the circuit (Figure 6a) for resistance values typical of different voltage levels and different lengths of transmission line.

voltage systems (as described above), it can be seen that GIC values initially increase with increasing line length, but for longer line lengths GIC values approach a constant value given by the electric field divided by the line resistance per unit length. Several studies have focused on line length as a risk factor for GIC. However, GIC do not necessarily flow to or from ground at the ends of a long line if this is part of a larger network that allows the GIC to keep flowing on other transmission lines. Instead, GIC typically flow to/from ground through substations at the edge of a network: the well-known "edge effect." Thus, the important characteristic is the "system length" rather than the length of any individual line.

Locations where the largest GIC flow to ground also depend on the direction of the electric field. This can easily be examined by modeling GIC for a uniform electric field in the northward and eastward directions. This gives a set of GIC reference values that can be combined to give the GIC produced by an electric field in any direction, θ, rotated clockwise from north [*Boteler*, 2013]:

$$i_k = \alpha_k |E| \cos(\theta) + \beta_k |E| \sin(\theta) \tag{29}$$

where α_k are obtained by calculating i_k for case $E_N = 1$ V/km, and $E_E = 0$, β_k are obtained by calculating i_k for $E_N = 0$ and $E_E = 1$ V/km.

Calculations can also be made [see *Arajärvi et al.*, 2011; *Boteler*, 2013] for the maximum values of GIC for a specified electric field amplitude as well as the directions of electric field producing the maximum values:

$$i_k(\text{peak}) = \sqrt{\alpha_k^2 + \beta_k^2}\ |E| \tag{30}$$

and

$$\theta_k(\text{peak}) = \tan^{-1} \frac{\beta_k}{\alpha_k} \tag{31}$$

Different substations, because of their place in a network, have their maximum sensitivity to GIC produced by different directions of a uniform electric field (see Figure 7). A good example of this, for the power system in Spain, is shown in Figure 5 of *Torta et al.* [2014]. Each system will have its own sensitivity dependent on its particular characteristics.

5. Geomagnetic Source Fields

For modeling GIC the important aspects of geomagnetic disturbances are the amplitude, frequency content, and spatial characteristics of the disturbance. Different types of disturbance have different spatial and temporal features [see *Viljanen*, 2012; *Boteler*, 2015a, and references therein]. The magnetic storm main phase is produced by a ring current in the radiation belt 4–6 Earth radii (R_E) above the Earth's surface and produces large-scale disturbances that can be reasonably considered as a uniform source. In contrast, magnetic

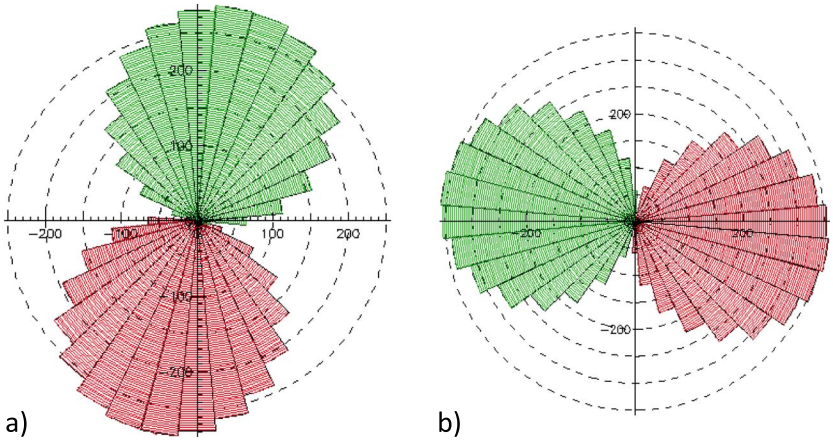

Figure 7. Directional sensitivity for (a) substation 5 and (b) substation 6 in the benchmark model of *Horton et al.* [2012].

substorms are produced by field-aligned currents and an ionospheric current that is only 100 km above the Earth's surface producing a localized disturbance. Other disturbances can contain a combination of sources: a storm sudden commencement (SSC) has traditionally been attributed to magnetopause currents, approximately 10 R_E above the Earth, but *Fiori et al.* [2014] have shown that some SSC signatures on the ground feature a high-latitude enhancement due to ionospheric currents. Thus, for modeling GIC there is a need to be able to include both large-scale and small-scale magnetic source fields due to distant (magnetospheric) and nearby (ionospheric) currents, respectively.

5.1. Magnetospheric Sources

For large-scale magnetic fields, produced by distant magnetospheric currents, it is reasonable to treat the source field as uniform across the region of interest, i.e., the area of the power system. The electric field can then be calculated using the amplitudes and frequencies of the magnetic disturbance and the transfer function of the Earth. In the frequency domain the Earth transfer function can be written as a relationship between $E(\omega)$ and $B(\omega)$ or between $E(\omega)$ and $g(\omega)$ where $g(t) = \mathrm{d}B(t)/\mathrm{d}t$.

$$E(\omega) = K(\omega)B(\omega) \tag{32}$$

$$E(\omega) = C(\omega)g(\omega) \tag{33}$$

These transfer functions are analogous to "high-pass" and "low-pass" filters, respectively.

5.2. Ionospheric Sources

Calculations can be made [e.g., *Häkkinen and Pirjola*, 1986] for the electric and magnetic fields produced at the surface of a layered Earth by a general model of ionospheric and field-aligned currents. However, the numerical integrations are computationally demanding and there is generally insufficient information about the current systems for these methods to be used for GIC applications. Instead, various simpler approximate techniques have been developed that provide sufficient accuracy when compared to the accuracy with which the ionospheric currents are known and are more easily incorporated into GIC modeling.

The auroral electrojet can be represented, to a first approximation, by a line current at a height, $h = 100$ km. The magnetic field variations generated by this current induce electric currents in the Earth, and these induced currents also contribute to the magnetic and electric fields at the Earth's surface. The influence of the induced currents can be well represented by an image current at a complex depth $h + p$ where p is the complex skin depth in the Earth [*Boteler and Pirjola*, 1998b]. The electric field is then given by

$$E(\omega) = -\frac{j\omega\mu_0 I}{2\pi}\ln\left[\frac{\sqrt{(h+2p)^2+x^2}}{\sqrt{h^2+x^2}}\right] \tag{34}$$

where x is the horizontal distance from the location of the electrojet. A real auroral electrojet does not have this idealized structure, but this approach provides the basis for modeling more realistic current systems. The auroral electrojet typically extends over 5–6° of latitude and may be composed of several current filaments. If

the electrojet current density is assumed to be at a height h and have a Cauchy distribution with half width, a, then the magnetic and electric fields produced are the same as the fields produced by a line current at a height $h+a$ [*Boteler et al*., 2000]. This allows the electric fields to be calculated by a simple modification of the above equation to give

$$E(\omega) = -\frac{j\omega\mu_0 I}{2\pi} \ln\left[\frac{\sqrt{(h+a+2p)^2+x^2}}{\sqrt{(h+a)^2+x^2}}\right] \tag{35}$$

Pirjola and Viljanen [1998] extended the use of the complex image method (CIM) to the case of a "U-shaped" current, which consists of a horizontal line current of finite length together with vertical upward currents at the ends. The vertical currents simulate field-aligned currents at high latitudes. The extension is based on the facts that CIM works for any horizontal current system and that a vertical current is equivalent to a horizontal current distribution regarding the magnetic field and the horizontal electric field at the Earth's surface. The length of the horizontal part of the U-shaped current can have any value, so the current can represent an electrojet of finite length as well as be a current element at an ionospheric grid point. The latter enables the CIM modeling to be used for any ionospheric current system including, for example, a westward traveling surge [*Pirjola et al*., 2000].

5.3. Use of Magnetic Observatory Data

The plane wave calculations can be made using time series data from magnetic observatory recordings. If magnetic data is only available from one observatory in the area of a particular power system, then using this data for calculations across the whole power system involves the implicit assumption that the magnetic field variations are spatially uniform across the power system. If data are available from two magnetic observatories, at opposite ends of a power system, then the magnetic field variations at sites across the power system can be approximated by linear interpolation from the observatory recordings [*Boteler*, 2014]. In both these cases there may be spatial structure in the source fields such that a uniform or linear approximation is not valid. When these approximations are used it is not because they can always be justified: rather, it is because they are the best that can be done with the data that is available.

To improve GIC modeling by including spatial variability in the magnetic source fields requires use of more magnetic recordings sites in the area of a power system. In some areas, magnetometer chains operated for academic research [*Viljanen and Häkkinen*, 1997; *Mann et al*., 2008; *Connors et al*., 2016] can be utilized and the power industry (EPRI/DoE and HydroOne) is installing extra magnetometers to improve the coverage in their areas. Where there are magnetic data from multiple sites it is necessary to use an interpolation scheme to provide magnetic field values across the whole region of the power system. The areas involved can be large enough so that the Earth's surface cannot be assumed to be planar and spherical schemes such as spherical elementary current system method [*Amm and Viljanen*, 1999; *Viljanen et al*., 2004] and spherical cap harmonic analysis [*Haines*, 1985; *Haines and Torta*, 1994] should be used.

6. Earth Conductivity Structure

Earth conductivity structure has an important influence on GIC and needs to be included in GIC modeling. Information on Earth conductivity is derived from magnetotelluric surveys involving colocated measurements of magnetic and electric fields [see *Simpson and Bahr*, 2005, and references therein]. There is an extensive literature on the magnetotelluric technique and the Earth conductivity structure, including papers in this special issue. It is not the purpose here to replicate any of that: rather, this section examines the type of information available and how it can be used in GIC modeling.

The Earth has a three-dimensional (3-D) conductivity structure, but because of lack of information or limitations in modeling techniques, many GIC studies have used simplified models. We show here how 1-D Earth conductivity structure is being used in GIC modeling before considering how 2-D/3-D structure can be utilized.

6.1. One-Dimensional Models

One-dimensional conductivity models consist of a set of horizontal layers with different conductivities chosen to reproduce the conductivity variation with depth within the Earth. The Earth consists of the crust

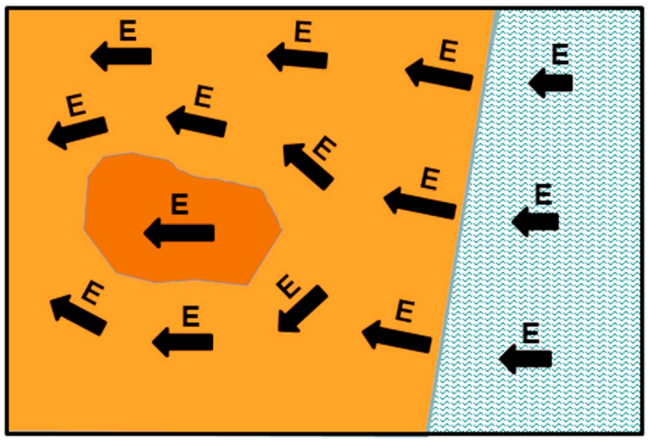

Figure 8. Deflection of electric fields by 2-D/3-D Earth conductivity structure such as due to a high-resistivity geological region (dark brown) or a coastline.

above the mantle and core. The crust and upper mantle have a lower conductivity, but with increasing temperature and pressure at greater depths partial melting of the rocks starts to occur leading to higher conductivities. The geomagnetic field variations with periods of concern for GIC (1 s to 24 h) have skin depths that extend, at the longest periods, down into the core. Therefore, the conductivity structure down to these depths has to be taken into account in calculating the electric fields that drive GIC. This can be done by using a recursive calculation of the response of the bottom layer that is then used as the terminating impedance for calculations for the next layer, and so on, to give the transfer function at the surface of the Earth [*Weaver*, 1994; *Trichtchenko and Boteler*, 2002]. This transfer function applies for fields in any direction so the same transfer function, $K(\omega)$ is used for calculations using the northward (x) and eastward (y) components of the electric field

$$E_x(\omega) = K(\omega)B_y(\omega) \tag{36}$$

$$E_y(\omega) = -K(\omega)B_x(\omega) \tag{37}$$

and the electric field is always orthogonal to the magnetic field variations.

These 1-D models ignore lateral variations in the Earth conductivity structure. However, different 1-D models have been constructed for different regions, so GIC modeling for a particular power system would use the 1-D model for the area of that power system. Even within the area of one power system a piecewise approach can be used with different 1-D models to provide an approximate way of taking account of lateral changes in the Earth conductivity structure [*Marti et al*., 2014a].

6.2. Two-Dimensional/Three-Dimensional Models

Two-dimensional and three-dimensional Earth conductivity structure introduces some features not seen with 1-D models. First, the Earth transfer function may not be the same for all directions, i.e., $K_{yx} \neq K_{xy}$. The second factor, illustrated in Figure 8, is that the electric fields are deflected by conductivity changes produced by geologic zones or boundaries such as at a coastline. Thus, the electric field is not always orthogonal to the magnetic field variations.

For example, consider a northward magnetic field variation that will produce an induced electric field that is dominantly westward but in the vicinity of conductivity changes may be deflected to have a northward or southward component. This is accounted for by introducing Earth transfer functions K_{xx} and K_{yy}. Thus, the general expressions for electric fields at the surface of a 2-D or 3-D Earth are

$$E_x(\omega) = K_{xx}(\omega)B_x(\omega) + K_{xy}(\omega)B_y(\omega) \tag{38}$$

$$E_y(\omega) = K_{yx}(\omega)B_x(\omega) + K_{yy}(\omega)B_y(\omega) \tag{39}$$

6.3. Source of Earth Conductivity Information

For GIC modeling we need the Earth transfer function relating the electric field components, E_x and E_y to the magnetic field components, B_x and B_y as shown in equations (36) and (37) or equations (38) and (39). Much of the magnetotelluric literature presents information in terms of the "surface impedance," $Z(\omega)$ relating E and H, or between E and dB/dt, sometimes referred to as the magnetotelluric relation, $C(\omega)$, but these are easily used to give the transfer function, $K(\omega)$:

$$K(\omega) = \frac{Z(\omega)}{\mu_0} = \frac{C(\omega)}{i\omega} \tag{40}$$

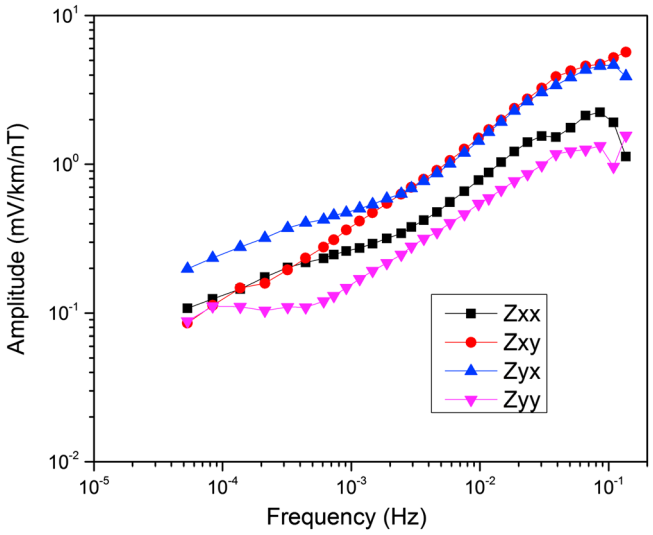

Figure 9. Magnetotelluric tensor impedances determined from measurements at Lost Creek Lake (plotted from data provided on the Earthscope web page: http://ds.iris.edu/spud/emtf/1425998).

Transfer function values can be obtained directly from measurements, such as those from the Earthscope project (http://www.usarray.org/researchers/obs/magnetotelluric), where these are available. These measurements provide surface impedance values at a set number of frequencies, and values at intervening frequencies can be determined by linear interpolation between pairs of measured values. Figure 9 shows an example of surface impedances from the Earthscope site at Lost Creek Lake (http://ds.iris.edu/spud/emtf/1425998).

However, many power systems cover areas where there may be no or limited magnetotelluric results available. In such cases, it may be possible to extrapolate magnetotelluric (MT) results from neighboring areas within the same geological terrain. The surface impedances then need to be calculated using models of the Earth conductivity structure. There are a variety of modeling techniques (see overview by *Dong et al*. [2013]) such as finite difference, finite element, and thin sheet methods that can be used. All techniques involve approximating the conductivity structure by a gridded model and making calculations at the grid points, with grid spacings to be used for different frequencies chosen following the guidelines of *Weaver* [1994] and reproduced in *Simpson and Bahr* [2005]. With this the modeling can be done for the whole range of frequencies to generate model values for the tensor impedances similar to those shown in Figure 9.

To use these impedance estimates to calculate electric fields, a set of magnetic field data (e.g., 1 day) can be Fourier transformed to give the corresponding magnetic field spectrum at a range of frequencies determined by the duration and sampling rate of the data set. For each of these frequencies the magnetic field spectral value is multiplied by the corresponding Earth transfer function value to give the electric field spectrum. An inverse Fourier transform is then used to give the electric field variations in the time domain. The impedance estimates derived from magnetotelluric measurements have some uncertainties associated with them, and these carry over to the Earth models derived from them. Therefore, whether using impedance obtained directly from measurements or from models, it is important to study the error bars and how they affect the electric fields calculated using these impedance values. Examples of how uncertainties in Earth models affect the calculated electric fields are provided by *Boteler* [2015b].

6.4. Time Domain Relations

For some applications it is preferable to calculate the electric field in the time domain by convolution of the magnetic field with the impulse response of the Earth, $K(t)$, or convolution between the rate of change of the magnetic field and the step response of the Earth, $C(t)$.

$$E(t) = K(t) \otimes B(t) \tag{41}$$

$$E(t) = C(t) \otimes \mathrm{d}B(t)/\mathrm{d}t \tag{42}$$

where, by the differential theorem of convolution

$$K(t) = \mathrm{d}C(t)/\mathrm{d}t \tag{43}$$

The impulse response and transfer function pair are related by a Fourier transform, as are the step response and magnetotelluric relation. For a uniform Earth (with conductivity, σ) the expression for the magnetotelluric relation (6) allows an analytic transform [*Bracewell*, 1978] to give the step response

$$c(t) = \frac{1}{\sqrt{\pi \mu_0 \sigma}} t^{-1/2} \Theta(t) \tag{44}$$

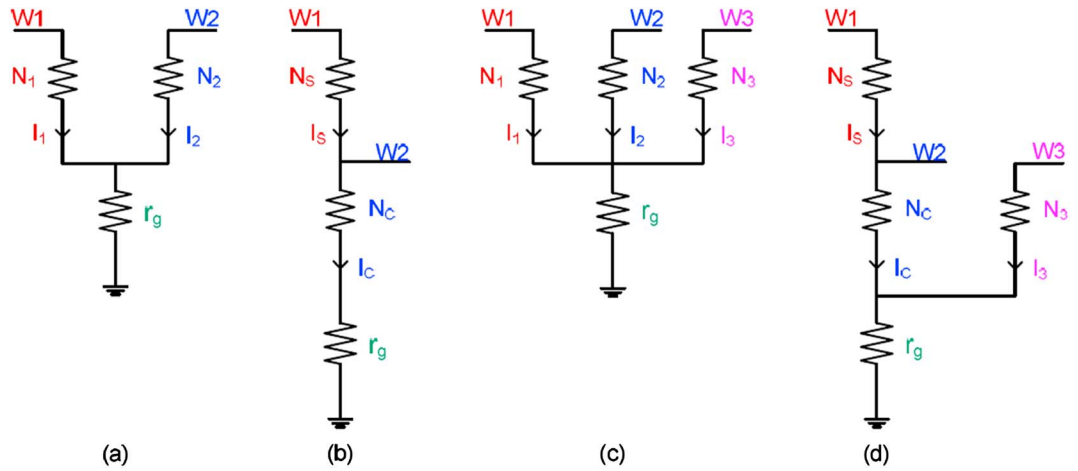

Figure 10. Effective GIC calculation for various transformers [from *Patil*, 2014]. (a) Two-winding. (b) Two-winding auto. (c) Three-winding. (d) Three-winding auto.

where Θ is the Heaviside function

$$\begin{aligned} \Theta(t) &= 1 \quad t > 0 \\ \Theta(t) &= 0 \quad t < 0 \end{aligned} \tag{45}$$

For a layered Earth the magnetotelluric relation, C, can be fitted with a rational function,

$$C(\omega) = C_0 \frac{(j\omega + z_1)(j\omega + z_2) \ldots (j\omega + z_n)}{(j\omega + p_1)(j\omega + p_2)\ldots(j\omega + p_n)} \tag{46}$$

which can be written

$$C(\omega) = k_0 + \sum_{i=1}^{n} \frac{k_i}{j\omega + p_i} \tag{47}$$

where each term has an analytic transform to give an impulse response as a summation of exponential terms:

$$c(t) = k_0 + \sum_{i=1}^{n} k_i \cdot e^{-p_i t} \tag{48}$$

These allow the convolution to be calculated using a recursive algorithm, thus providing an efficient method for real-time calculation of electric fields for use in GIC modeling [*Marti et al*., 2014b]. This approach is being explored to see if it can be applied to any transfer functions, such as functions derived from measurements as in Figure 9 or from 2-D or 3-D modeling.

7. Discussion

GIC modeling is just part of the wider problem of geomagnetic effects on power systems [*Pirjola*, 2012; *Boteler*, 2015a; *Pulkkinen et al*., 2016]. The previous sections look at the factors that need to be taken into account in order to model GIC. However, it is also necessary to consider the ways in which GIC modeling is used. The main application is to determine whether the GIC that occur under specified space weather conditions are large enough to produce detrimental effects on system components, particularly transformers, or on the operation of the power system itself. The former requires modeling of the transformer heating produced by GIC [e.g., *Marti et al*., 2013a]. The main concern with regard to system operation is the increased reactive power demand of transformer affected by GIC, and a number of studies are now combining GIC modeling with reactive power calculations to assess system stability [*Jacobson et al*., 2014; *Gérin-Lajoie et al*., 2014].

For assessing the impact of GIC on transformers, it is important to consider the GIC in all transformer windings. *Albertson et al*. [1981] introduced an "effective GIC" to take account of different GIC values in the series and common windings of an autotransformer. *Zheng et al*. [2014] showed that an equivalent formula also applies to two-winding transformers. *Patil* [2014] has now extended the calculation of effective GIC to three-winding transformers. The expressions for effective GIC can look quite different depending on the

choice of turns ratio used by the different authors. However, these can all be represented in a standard format. Consider the transformers with different winding configurations shown in Figure 10. In each case we calculate the effective GIC as the GIC flowing from the high voltage level, W1, to ground that would produce the same magnetic flux in the core as the combination of GIC in all the windings.

Then equating fluxes for the transformer in Figure 10a gives

$$I_1 N_1 + I_2 N_2 = I_{\text{eff}} N_1 \tag{49}$$

which gives the effective GIC for a two-winding transformer:

$$I_{\text{eff}} = I_1 \frac{N_1}{N_1} + I_2 \frac{N_2}{N_1} \tag{50}$$

The same approach for a three-winding transformer (Figure 10c) gives

$$I_{\text{eff}} = I_1 \frac{N_1}{N_1} + I_2 \frac{N_2}{N_1} + I_3 \frac{N_3}{N_1} \tag{51}$$

Equating fluxes for the autotransformer in Figure 10b gives

$$I_S N_S + I_C N_C = I_{\text{eff}} (N_S + N_C) \tag{52}$$

which gives the effective GIC for a two-winding autotransformer

$$I_{\text{eff}} = I_S \frac{N_S}{N_S + N_C} + I_C \frac{N_C}{N_S + N_C} \tag{53}$$

A similar expression is obtained for the three-winding autotransformer (Figure 10d):

$$I_{\text{eff}} = I_S \frac{N_S}{N_S + N_C} + I_C \frac{N_C}{N_S + N_C} + I_3 \frac{N_3}{N_S + N_C} \tag{54}$$

It can be seen that all the formulas for effective GIC have a common format with the current in each winding multiplied by the number of turns for that winding and divided by the number of turns for the windings where the effective GIC is considered to flow. By appropriate algebra these formulas can be converted into the forms used by *Albertson et al*. [1981], *Zheng et al*. [2014], and *Patil* [2014].

An issue, often overlooked in GIC modeling, is whether there are any effects from transformer inductances on GIC. This is opposite to the concerns about GIC effects on transformers. At the start of the descriptions of GIC modeling above it was stated that at the frequencies normally considered in GIC studies, the reactive impedances are assumed to be negligible and power systems can be modeled as a network of resistances. This has been the assumption (often unstated) in almost all GIC model calculations. Any delays in GIC growth were not considered significant as it was the final steady state GIC values that were required. When GIC calculations started to be made with electric fields calculated from magnetic data, the standard cadence for the magnetic recordings and hence the calculated electric field values was 1 sample/min, so delays in GIC growth of the order of seconds were of no consequence.

Now the situation is different. Power systems are utilizing high-voltage transmission lines, with lower resistances, R, connected to larger transformers, with high inductances, L, so the L/R time constants of the power system are getting longer. Also, as we go to higher sampling rates for magnetic data (the new INTERMAGNET standard for magnetic observatories is 1 sample/s) there will be higher frequencies in the calculated electric fields used as inputs for GIC modeling. Power system time constants of the order of seconds could now have a significant effect on the higher-frequency content of GIC.

Calculating the growth of GIC following a step in applied voltage is not a trivial task. It cannot be treated as a simple L-R circuit calculation because the inductance of the transformer changes every cycle as it goes in and out of saturation. Transient analysis programs such as Electromagnetic Transients Program [*Dommel*, 1993] can be used but require short time steps that can follow the AC waveform as over many cycles. This led to methods for speeding up the calculations and the development of formulas for calculating the time for a transformer to saturate [*Bolduc and Kieffer*, 1992; *Bolduc et al*., 2000]. An alternative approach is to calculate an "effective inductance" that depends on the fraction of time a transformer is in saturation [*Boteler*, 1994]. This provides a much simpler way to model the growth in GIC that gives the same results as the transient analysis calculations [*Boteler and Bradley*, 2016]. A further complicating factor is that many transformers have

delta windings and currents circulating in these windings delay the saturation of the transformer [*Walling*, 2014]. All these factors mean that the transformers act to slow the growth of GIC: the exact time constants involved will depend on the specific characteristics of the transformers and the wider power system circuit for GIC flow and need further research. However, the overall effect of transformer inductances on GIC is to damp out the fastest variations; thus, GIC values calculated using a purely resistive model of a power system will represent an upper limit for the GIC values that would be obtained in practice.

8. Conclusions

GIC modeling has evolved considerably from calculations with a fixed electric field value as input to a model representing only the highest voltage level in a power system to modeling that takes account of geomagnetic disturbance characteristics and Earth conductivity to calculate time-varying GIC in multiple voltage levels of a power system.

Modeling GIC flow within a substation has required a change in thinking about the model. Only including a single voltage level allowed the high-voltage bus at a substation to be designated as a node in the model, and the transformers at that substation were combined to give a single resistance to ground from that node; while transmission lines between substations were represented as branches connecting nodes in the network and were exposed to the geoelectric field. Now including multiple voltage levels with a node at each one as well as nodes at neutral points, the only grounded nodes in the network are the ground mats at each substation. All of the rest of the connections are branches: some of these are transformer windings and other connections within a substation, while some are transmission lines connecting between substations. It is only the branches that are transmission lines that experience the geoelectric fields.

Geomagnetic disturbances can be modeled, depending on their spatial characteristics, as a plane wave or as a combination of magnetic fields due to line current segments, and formulas are available for calculating the electric fields produced by the source fields using simple Earth conductivity models. Alternatively, recorded magnetic observatory data can be used, either directly or with a suitable interpolation scheme, to calculate the electric fields across a power system. The limiting factor in some cases is the lack of sufficient magnetometer installations to provide full information about the spatial variation of the geomagnetic field fluctuations.

Earth conductivity information is necessary to provide the Earth transfer functions that enable calculations of the electric fields to be used as inputs in the GIC modeling. Where they are available, Earth transfer functions can be obtained directly from magnetotelluric (MT) measurements. Alternatively, knowledge of the geologic terrains and extrapolation of MT results can be used to build up 1-D models of different regions that can easily be used in GIC modeling. However, the Earth has a 3-D conductivity structure and more work is needed to develop 2-D and 3-D models that can easily be incorporated into GIC modeling.

GIC modeling itself has reached a high state of application readiness. As shown in this paper, the GIC modeling can incorporate information on the geomagnetic disturbance characteristics and on the 3-D Earth conductivity structure. The limiting factor is the availability of sufficient information on the geomagnetic disturbances and the Earth conductivity. However, steps are being taken to address these information gaps. Software implementations of GIC modeling are being developed to provide the tools for geomagnetic hazard assessments being required by new industry rules, and real-time modeling of GIC [*Marti et al.*, 2013b] is already being used in a power system control center as part of geomagnetic disturbance management.

Acknowledgments
We are grateful to the reviewers for their detailed reading of the manuscript and useful comments. The data used are listed in the references, tables, supplements, and Earthscope repository at http://ds.iris.edu/spud/emtf/1425998. Figure 10 is reprinted with permission from CIGRE Paper C4-306, Patil, K., Modeling and Evaluation of Geomagnetic Storms in the Electric Power System, © 2014.

References

Albertson, V. D., J. G. Kappenman, N. Mohan, and G. A. Skarbakka (1981), Load-flow studies in the presence of geomagnetically-induced currents, *IEEE Trans. Power Appar. Syst.*, *PAS-100*, 594–606.

Amm, O., and A. Viljanen (1999), Ionospheric disturbance magnetic field continuation from the ground to the ionosphere using spherical elementary current systems, *Earth Planets Space*, *51*, 431–440.

Arajärvi, E., and A. Viljanen (2008), Geomagnetically induced current estimation in the Wisconsin 345-kV power grid, *Rep. 1018125*, EPRI, Palo Alto, Calif.

Arajärvi, E., R. Pirjola, and A. Viljanen (2011), Effects of neutral point reactors and series capacitors on geomagnetically induced currents in a high-voltage electric power transmission system, *Space Weather*, *9*, S11005, doi:10.1029/2011SW000715.

Barbosa, C. S., G. A. Hartmann, and K. J. Pinheiro (2015), Numerical modeling of geomagnetically induced currents in a Brazilian transmission line, *Adv. Space Res.*, *55*(4), 1168–1179, doi:10.1016/j.asr.2014.11.008.

Bernabeu, E. E. (2013), Modeling geomagnetically induced currents in Dominion Virginia Power using extreme 100-year geoelectric field scenarios—Part 1, *IEEE Trans. Power Delivery*, *28*, 516–523.
Bernhardi, E. H., P. J. Cilliers, and C. T. Gaunt (2008), Improvement in the modelling of geomagnetically induced currents in southern Africa, *S. Afr. J. Sci.*, *104*(7–8), 265–272.
Bolduc, L., and P. Kieffer (1992), A recipe for fast simulation of the effect of the DC component of magnetizing steady-state currents in transformers using EMTP, in *Proceedings Geomagnetically Induced Currents Conference, Milbrae, California, November 8–10, 1989*, 24-1–24-8, TR-100450, EPRI, Palo Alto.
Bolduc, L., A. Gardreau, and A. Dutil (2000), Saturation time of transformers under DC excitation, *Electr. Power Syst. Res.*, *56*, 95–102.
Boteler, D. H. (1994), Characteristics of time-varying inductance, *IEEE Trans. Magn.*, *30*, 172–176.
Boteler, D. H. (1999), Calculating the voltages induced in technological systems during a geomagnetic disturbance, *IEEE Trans. Electromagn. Compat.*, *41*, 398–402.
Boteler, D. H. (2013), The use of linear superposition in modelling geomagnetically induced currents, paper 001545 presented at IEEE Power & Energy Society General Meeting, Vancouver, 21–15 July.
Boteler, D. H. (2014), Methodology for simulation of geomagnetically induced currents in power systems, *J. Space Weather Space Clim.*, *4*, A21, doi:10.1051/swsc/2014018.
Boteler, D. H. (2015a), The impact of space weather on the electric power grid, in *Heliophysics V. Space Weather and Society, Early Chap. Collect. V. Jan. 5, 2015*, edited by C. J. Schrijver, F. Bagenal, and J. J. Sojka, pp. 74–95, UCAR, Boulder, Colo. [Available at http://www.lmsal.com/~schryver/HSS5/HSS5.pdf.]
Boteler, D. H. (2015b), The evolution of Québec Earth models used in modelling geomagnetically induced currents, *IEEE Trans. Power Delivery*, *30*(5), 2171–2178.
Boteler, D. H., and E. Bradley (2016), On the interaction of power transformers and geomagnetically induced currents, *IEEE Trans. Power Delivery*, doi:10.1109/TPWRD.2016.2576400.
Boteler, D. H., and R. J. Pirjola (1997), Nature of the geoelectric field associated with GIC in long conductors such as power systems, pipelines, and phone cables, in *Proceedings of the Beijing EMC Symposium, May 1997*, pp. 68–71, Beijing University, Beijing.
Boteler, D. H., and R. J. Pirjola (1998a), Modelling geomagnetically induced currents produced by realistic and uniform electric fields, *IEEE Trans. Power Delivery*, *13*, 1303–1308.
Boteler, D. H., and R. J. Pirjola (1998b), The complex image method for calculating the magnetic and electric fields produced at the surface of the Earth by the auroral electrojet, *Geophys. J. Int.*, *132*, 31–40.
Boteler, D. H., and R. J. Pirjola (2014), Comparison of methods for modelling geomagnetically induced currents, *Ann. Geophys.*, *32*, 1177–1187, doi:10.5194/angeo-32-1177-2014.
Boteler, D. H., Q. Bui-Van, and J. Lemay (1994), Directional sensitivity to geomagnetically induced currents of the Hydro-Quebec 735 kV power system, *IEEE Trans. Power Delivery*, *9*, 1963–1971.
Boteler, D. H., R. Pirjola, and L. Trichtchenko (2000), On calculating the magnetic and electric fields produced at the Earth's surface by a "wide" electrojet, *J. Atmos. Sol. Terr. Phys.*, *62*, 1311–1315.
Boteler, D. H., A. J. C. Lackey, L. Marti, and S. Shelemy (2013), Equivalent circuits for modelling geomagnetically induced currents from a neighbouring network, paper 002195 presented at IEEE Power & Energy Society GM, Vancouver, 21–25 July.
Bracewell, R. N. (1978), *The Fourier Transform and Its Applications*, 2nd ed., McGraw-Hill, New York.
Caraballo, R., L. Sánchez Bettucci, and G. Tancredi (2013), Geomagnetically induced currents in the Uruguayan high-voltage power grid, *Geophys. J. Int.*, *195*, 844–853.
Connors, M., I. Schofield, K. Reiter, P. J. Chi, K. M. Rowe, and C. T. Russell (2016), The AUTUMNX magnetometer meridian chain in Québec, Canada, *Earth Planets Space*, *68*, 2, doi:10.1186/s40623-015-0354-4.
Dommel, H. (1993), *Electromagnetic Transients Program (EMTP) Theory Book*, Bonneville Power Admin., Portland, Oreg.
Dong, B., Z. Wang, R. Pirjola, and D. Boteler (2013), Review of Earth conductivity structure modeling techniques in different dimensions, paper 000296 presented at IEEE Power & Energy Society General Meeting, Vancouver, 21–15 July.
Erinmez, I. A., J. G. Kappenman, and W. A. Radasky (2002), Management of the geomagnetically induced current risks on the national grid company's electric power transmission system, *J. Atmos. Sol. Terr. Phys.*, *64*(5–6), 743–756.
Fiori, R. A. D., D. H. Boteler, and D. M. Gillies (2014), Assessment of GIC risk due to geomagnetic sudden commencements and identification of the current systems responsible, *Space Weather*, *12*, 76–91, doi:10.1002/2013SW000967.
Gérin-Lajoie, L., J. Mahseredjian, S. Guillon, and O. Saad (2014), Simulation of voltage collapse caused by GMDs—Problems and solutions, paper C4-301 presented at CIGRE 2014.
Gilbert, J. L., W. A. Radasky, and E. B. Savage (2012), A technique for calculating the currents induced by geomagnetic storms on large high voltage power grids, in *Proceedings of the 2012 IEEE International Symposium on Electromagnetic Compatibility (EMC), 6–10 August, 2012*, pp. 323–328, IEEE, New York.
Guo, S.-X., L.-G. Liu, R. J. Pirjola, K.-R. Wang, and B. Dong (2015), Impact of the EHV power system on geomagnetically induced currents in the UHV power system, *IEEE Trans. Power Delivery*, *30*(5), 2163–2170, doi:10.1109/TPWRD.2014.2381248.
Haines, G. V. (1985), Spherical cap harmonic analysis, *J. Geophys. Res.*, *90*, 2583–2591, doi:10.1029/JB090iB03p02583.
Haines, G. V., and J. M. Torta (1994), Determination of equivalent current sources from spherical cap harmonic models of geomagnetic field variations, *Geophys. J. Int.*, *118*(3), 499–514.
Häkkinen, L., and R. Pirjola (1986), Calculation of electric and magnetic fields due to an electrojet current system above a layered Earth, *Geophysica*, *22*(31–44), 3–32.
Horton, R., D. H. Boteler, T. J. Overbye, R. J. Pirjola, and R. Dugan (2012), A test case for the calculation of geomagnetically induced currents, *IEEE Trans. Power Delivery*, *27*(4), 2368–2373.
Jacobson, D. A. N., S. Shelemy, W. Chandrasena, D. Boteler, and R. Pirjola (2014), Development of advanced GIC analysis tools for the Manitoba power grid, paper C4-302, paper presented at CIGRE Session 45, Paris, 24–29 Aug.
Kappenman, J. G. (2007), Geomagnetic disturbances and impacts upon power system operation, in *The Electric Power Engineering Handbook*, 2nd ed., edited by L. L. Grigsby, chap. 16, pp. 16-1–16–22, CRC Press/IEEE Press, Boca Raton, Fla.
Kappenman, J. G., V. D. Albertson, and N. Mohan (1981), Investigation of geomagnetically induced currents in the proposed Winnipeg-Duluth-Twin Cities 500-kV transmission line *Final Rep. for Res. Proj. 1205-1*, prepared for Electric Power Res. Inst. (EPRI), Palo Alto, July.
Kelly, G. S., A. Viljanen, C. D. Beggan, A. W. P. Thomson, and A. Ruffenach (2016), Understanding GIC in the UK and French high voltage transmission systems during severe magnetic storms, *Space Weather*, doi:10.1002/2016SW001469.
Koen, J. (2002), Geomagnetically induced currents in the Southern African Electricity Transmission Network, PhD thesis, 202 pp., Univ. of Cape Town, Cape Town, South Africa.

Lehtinen, M., and R. Pirjola (1985), Currents produced in earthed conductor networks by geomagnetically-induced electric fields, *Ann. Geophys.*, *3*, 479–484.
Liu, C., Y. Li, and L. Chen (2013), Modelling geomagnetically induced currents in Xinjiang 750 kV power grid in China, in *Proceedings of the IEEE PES GM, Vancouver, July 2013*, pp. 1111–1115, IEEE, New York, doi:10.1109/PESMG.2013.6672378.
Liu, C., Y. Li, and R. Pirjola (2014), Observations and modeling of GIC in the Chinese large-scale high-voltage power networks, *J. Space Weather Space Clim.*, *4*, A03, doi:10.1051/swsc/2013057.
Mäkinen, T. (1993), *Geomagnetically Induced Currents in the Finnish Power Transmission System*, *Geophys. Publ. 32*, 101pp., Finnish Meteorol. Inst., Helsinki.
Mann, I. R., et al. (2008), The upgraded CARISMA magnetometer array in the THEMIS era, *Space Sci. Rev.*, *141*, 413–451, doi:10.1007/s11214-008-9457-6.
Marshall, R. A., E. A. Smith, M. J. Francis, C. L. Waters, and M. D. Sciffer (2011), A preliminary risk assessment of the Australian region power network to space weather, *Space Weather*, *9*, S10004, doi:10.1029/2011SW000685.
Marshall, R. A., M. Dalzell, C. L. Waters, P. Goldthorpe, and E. A. Smith (2012), Geomagnetically induced currents in the New Zealand power network, *Space Weather*, *10*, S08003, doi:10.1029/2012SW000806.
Marti, L., A. Rezaei-Zare, and A. Narang (2013a), Simulation of transformer hotspot heating due to geomagnetically induced currents, *IEEE Trans. Power Delivery*, *28*(1), 320–327.
Marti, L., A. Rezaei-Zare, and A. Yan (2013b), Modelling considerations for the Hydro One real-time GMD management system, in *Proceedings of the IEEE Power & Energy Society General Meeting, Vancouver, BC, 21–25 July 2013*, pp. 4126–4131, IEEE, New York, doi:10.1109/PESMG.2013.6673069.
Marti, L., C. Yiu, A. Rezaei-Zare, and D. Boteler (2014a), Simulation of geomagnetically induced currents with piecewise layered-Earth models, *IEEE Trans. Power Delivery*, *29*(4), 1886–1893.
Marti, L., A. Rezaei-Zare, and D. Boteler (2014b), Calculation of induced electric field during a geomagnetic storm using recursive convolution, *IEEE Trans. Power Delivery*, *29*(2), 802–807.
McKay, A. J. (2003), Geoelectric fields and geomagnetically induced currents in the United Kingdom, PhD thesis, Univ. Edinburgh.
Molinski, T. S. (2002), Why utilities respect geomagnetically induced currents, *J. Atmos. Sol. Terr. Phys.*, *64*(16), 1765–1778.
Myllys, M., A. Viljanen, Ø. A. Rui, and T. M. Ohnstad (2014), Geomagnetically induced currents in Norway: The northernmost high-voltage power grid in the world, *J. Space Weather Space Clim.*, *4*, A10, doi:10.1051/swsc/2014007.
Ngwira, C. M., A. Pulkkinen, L.-A. McKinnell, and P. J. Cilliers (2008), Improved modeling of geomagnetically induced currents in the South African power network, *Space Weather*, *6*, S11004, doi:10.1029/2008SW000408.
Patil, K. (2014), Modeling and evaluation of geomagnetic storms in the electric power system, paper C4-306 presented at CIGRE 2014, Paris.
Pirjola, R. (2005), Effects of space weather on high-latitude ground systems, *Adv. Space Res.*, *36*(12), 2231–2240, doi:10.1016/j.asr.2003.04.074.
Pirjola, R. (2012), Geomagnetically induced currents as ground effects of space weather, in *Space Science*, pp. 27–44, edited by H. J. Mosquera Cuesta, InTech, Rijeka, Croatia.
Pirjola, R., and M. Lehtinen (1985), Currents produced in the Finnish 400 kV power transmission grid and in the Finnish natural gas pipeline by geomagnetically-induced electric fields, *Ann. Geophys.*, *3*(4), 485–491.
Pirjola, R., and A. Viljanen (1998), Complex image method for calculating electric and magnetic fields produced by an auroral electrojet of a finite length, *Ann. Geophys.*, *16*, 1434–1444.
Pirjola, R., D. Boteler, A. Viljanen, and O. Amm (2000), Prediction of geomagnetically induced currents in power transmission systems, *Adv. Space Res.*, *26*(1), 5–14.
Pulkkinen, A., et al. (2016), Geomagnetically induced currents: Science, engineering and applications readiness, Space Weather, submitted.
Radasky, W. A., J. G. Kappenman, and J. L. Gilbert (2006), An overview of the development and validation of large power grid models for geomagnetic storms, in *Proceedings of the 2006 4th Asia-Pacific Conference on Environmental Electromagnetics, 1–4 August 2006*, pp. 25–28, IEEE, New York.
Simpson, F., and K. Bahr (2005), *Practical Magnetotellurics*, 254 pp., Cambridge Univ. Press, Cambridge, U. K.
Taylor, J., V. Singhvi, A. Tarditi, and M. Van Harte (2014), Application of geomagnetic disturbance vulnerability assessments using the Eskom Main Transmission System Model, paper C4-307 presented at CIGRE 2014.
Torta, J. M., S. Marsal, and M. Quintana (2014), Assessing the hazard from geomagnetically induced currents to the entire high-voltage power network in Spain, *Earth Planets Space*, *66*, 87, doi:10.1186/1880-5981-66-87.
Trichtchenko, L., and D. H. Boteler (2002), Modeling of geomagnetic induction in pipelines, *Ann. Geophys.*, *20*, 1063–1072.
Turnbull, K. (2010), Modelling GIC in the UK, *Astron. Geophys.*, *51*(5), 25–26, doi:10.1111/j.1468-4004.2010.51525.x.
Turnbull, K. (2011), Modelling of geomagnetically induced currents in the United Kingdom, PhD thesis, Univ. of Lancaster.
Viljanen, A. (2012), Description of the magnetospheric/ionospheric sources, in *The Magnetotelluric Method: Theory and Practice*, edited by A. D. Chave and A. G. Jones, chap. 3B, pp. 96–121, Cambridge Univ. Press, Cambridge, U. K.
Viljanen, A., and L. Häkkinen (1997), IMAGE magnetometer network, in *Satellite-Ground Based Coordination Sourcebook*, *ESA Publ.*, vol. SP-1198, edited by M. Lockwood, M. N. Wild, and H. J. Opgenoorth, pp. 111–117, ESA, Noordwijk.
Viljanen, A., A. Pulkkinen, O. Amm, R. Pirjola, T. Korja, and BEAR Working Group (2004), Fast computation of the geoelectric field using the method of elementary current systems and planar Earth models, *Ann. Geophys.*, *22*, 101–113.
Viljanen, A., R. Pirjola, M. Wik, A. Ádám, E. Prácser, Y. Sakharov, and J. Katkalov (2012), Continental scale modelling of geomagnetically induced currents, *J. Space Weather Space Clim.*, *2*, A17, doi:10.1051/swsc/2012017.
Viljanen, A., R. Pirjola, E. Pracser, J. Katkalov, and M. Wik (2014), Geomagnetically induced currents in Europe. Modelled occurrence in a continent-wide power grid, *J. Space Weather Space Clim.*, *4*, A09, doi:10.1051/swsc/2014006.
Walling, R. (2014), *Analysis of Geomagnetic Disturbance (GMD) Related Harmonics*, 3002002985, EPRI, Palo Alto, Calif.
Weaver, J. T. (1994), *Mathematical Methods for Geo-electromagnetic Induction*, Wiley, NewYork.
Wik, M., A. Viljanen, R. Pirjola, A. Pulkkinen, P. Wintoft, and H. Lundstedt (2008), Calculation of geomagnetically induced currents in the 400 kV power grid in southern Sweden, *Space Weather*, *6*, S07005, doi:10.1029/2007SW000343.
Zheng, K., L. G. Liu, H. Y. Ge, and W. X. Li (2012), Comparative study of the GIC amplitudes and characteristics in different power grids in China, paper C3-206 presented at CIGRE.
Zheng, K., D. H. Boteler, R. Pirjola, L. G. Liu, R. Becker, L. Marti, S. Boutilier, and S. Guillon (2014), Effects of system characteristics on geomagnetically induced currents, *IEEE Trans. Power Delivery*, *29*(2), 890–898.